

Molecular Dynamics Simulation of Hygroscopic Aging Effects in Epoxy Polymer

M. F. N. Taufique,^{a*} Martin Losada,^b Sebastien Hamel,^c Nir Goldman,^c Matthew J. DiTucci,^b
Loubna Pagnotti,^b Daniel Willis,^b Matthew Torres,^b Ram Devanathan^a

^a Pacific Northwest National Laboratory, Richland, WA 99354, United States

^b PPG Coatings Innovation Center, Allison Park, PA 15101, United States

^c Physical and Life Sciences Directorate, Lawrence Livermore National Laboratory,
Livermore, CA 94550, United States

*Corresponding author. Email: mohammadfn.taufique@pnnl.gov

Abstract: The automobile industry is incorporating more lightweight content in car designs to boost fuel-economy. New structural adhesives are needed to mitigate the corrosion and thermal expansion issues associated with joining dissimilar lightweight materials, but adhesive developers lack a fundamental understanding of the chemistry that occurs in the adhesive as the joint ages. In this study, we developed structural adhesive molecular models and applied classical molecular dynamics (MD) simulations and Density Functional Theory (DFT) calculations to gain molecular insights into the influence of water molecules on the properties of epoxy-based adhesives (DGEBA + Jeffamine (JD230)). The simulations were complemented by experimental synthesis and characterization. Our work underscores the impact of water molecules on the local structure of the epoxy network as well as resulting mechanical properties. Water molecules were mainly coordinated with hydroxyls, primary amines and secondary amines, but also weakly coordinated with ether linkages, which were found most probable to be labile. Simulated stress-strain data indicates that increasing the water content deteriorates the mechanical properties. The Young's modulus decreased by ~30% when the water content increased to 3 wt.%. This integration of molecular-level chemical insights with mechanical property simulations of the hydrated epoxy system and experimental validation holds the promise to advance lightweight joint technologies.

Introduction

Epoxy, a thermosetting polyepoxide with a 3-D network structure, is the product of the reaction between an epoxy resin and a curing agent such as a polyfunctional amine [1]. Epoxy has attracted a significant amount of attention in electronic packaging, aerospace and automobile industries due to its unique combination of properties, such as strength-to-weight ratio, high temperature resistance, low dielectric constant and processability [2-7]. Epoxy-based adhesives are being used as lightweight joints in automobiles to join dissimilar materials and improve the fuel efficiency. For instance, automobile parts such as body panels, powertrains, bumpers, exterior panels, chassis, brakes, instrument panels, tires, sensors, suspension, intake manifolds,

steering, leaf springs, fuel tanks, fuel cells, glazing, drive shafts, antiglare coatings, cross-vehicle beams, wheel covers, filters, valve covers, and other accessories are now being replaced with polymer nanocomposite materials [3, 4]. It has been estimated that 10–20 % reduction in the weight of the total vehicle improves the fuel economy by 5–10 % [5].

The mechanical and chemical properties of epoxy adhesives are strongly related to the functionality of the monomers, the molar ratio of epoxy and the curing agent, cross-linking density and distribution of the cross-linkers involved in the reaction [8-11]. The cross-linked structure of epoxy adhesives provides benefits in increased mechanical strength and makes them valuable in different industrial applications [12, 13]. On the other hand, the properties of the epoxy adhesives and their interfaces are sensitive to degradation when aging in the presence of moisture known as hygroscopic aging [14-17]. For instance, water uptake inside these epoxy adhesive matrices is a major concern. Hygroscopic aging in epoxy adhesives introduces complications such as interfacial delamination [18, 19], swelling [20, 21], plasticization [22] and induced corrosion [23, 24]. Therefore, epoxy degradation processes such as moisture-induced plasticization and the resulting rupture can strongly affect product performance over long timescales. Recently, extensive theoretical and experimental studies on epoxy adhesive polymers were carried out to study the fracture mechanics and moisture-assisted aging phenomena [25-31]. For instance, Choudhury et al. employed reactive force field (ReaxFF) to simulate the impact of molecular weight (MW) of cross-linkers and degree of cure and found that the lower MW cross-linker yields higher modulus and yield stress and reduced strain to failure and energy absorption than the higher MW cross-linkers [25]. To the best of our knowledge, a comprehensive study to integrate the atomic level information with large-scale experiments to find the root cause of hygroscopic aging during engineering application i.e in presence of mechanical load is missing. In order to make durable epoxy adhesives, it is essential to understand the interactions between the epoxy adhesive structure and water molecules and the resulting performance in terms of mechanical properties.

In the present work, we have performed classical molecular dynamics (MD) simulations and density functional theory (DFT) calculations with varied water content to mimic different states of hygroscopic aging. In addition to simulations, empirical characterization utilizing vibrational spectroscopy has been performed to investigate the adhesive-water interactions and their impact on mechanical properties. Our results from simulations and experiments indicate the presence of locally active sites for water association that can act as potential sites for scission during the early stages of hygroscopic aging in the presence of mechanical loads. Overall, the molecular modeling and experimental results presented in this study provide guidelines for understanding the complex hygroscopic aging effects in epoxy adhesives.

Methodology

Computational

We considered bisphenol A diglycidyl ether (DGEBA) epoxy with Jeffamine (JD230) curing agent as a model epoxy adhesive, presented in Figure 1 (a) and (b). A representative epoxy adhesive model was created by employing the COMPASS [32] force field with Materials Studio software [33]. Two different cross-linked (CL) epoxy networks, including 63% CL and 72% CL structures, were generated. To model the cross-linking process that usually occurs during the curing of the material, the following steps were taken to build the structure of the polymer:

(1) Geometry optimization of DGEBA and JD230 monomers was carried out using Materials Studio. The monomer optimized structures were randomly spread into a cell with the ratio of 2:1, respectively. We chose this ratio because every nitrogen atom has the potential to react with two ending carbons in the epoxy molecule. At this stage, 25 different configurations were generated and optimized. The configuration with the minimum total energy was chosen as the acceptable conformation for subsequent ambient temperature and pressure equilibration simulations using the NVT and NPT thermodynamic ensembles.

(2) Whenever the reactants from amine groups and epoxy rings came close to each other, the epoxy ring was opened and a bond was created between the nitrogen and the carbon to imitate the curing chemistry process. At the same time, the oxygen from the epoxy ring absorbs the hydrogen from the amine group to form the secondary hydroxyl group as presented in Figure 1 (c). In this regard, the minimum and maximum cut-off distances for creating the bond between carbon in the epoxy group and nitrogen in the amine group were 4 Å and 6 Å, respectively [34, 35]. The number of iterations in each radial distance was 5. All the crosslink simulations were carried out at 160° C and 1 atm pressure.

This process was iterated until either the maximum number of iterations was reached, or the algorithm could not find any possible pairs for bond creation. Thereafter, the cut-off distance was increased with a step size of 1 Å. The algorithm stopped the process when the maximum cut-off length was reached or when the desired degree of crosslinking was obtained. The crosslink percentages were calculated as the ratio of reacted atoms to the total of reactive atoms in the epoxy monomers. In this way, two cross-linked structures, 63% CL and 72% CL, were generated. The density of the equilibrated crosslinked structure and the glass transition temperature (T_g) were 1.10 g/cc and 88° C, respectively. The step-by-step techniques to equilibrate the crosslinked epoxy structures, density and T_g calculation are provided in Figures 1 and 2 in the supplementary section. These structures were further used to study the interactions with water molecules and resulting mechanical properties.

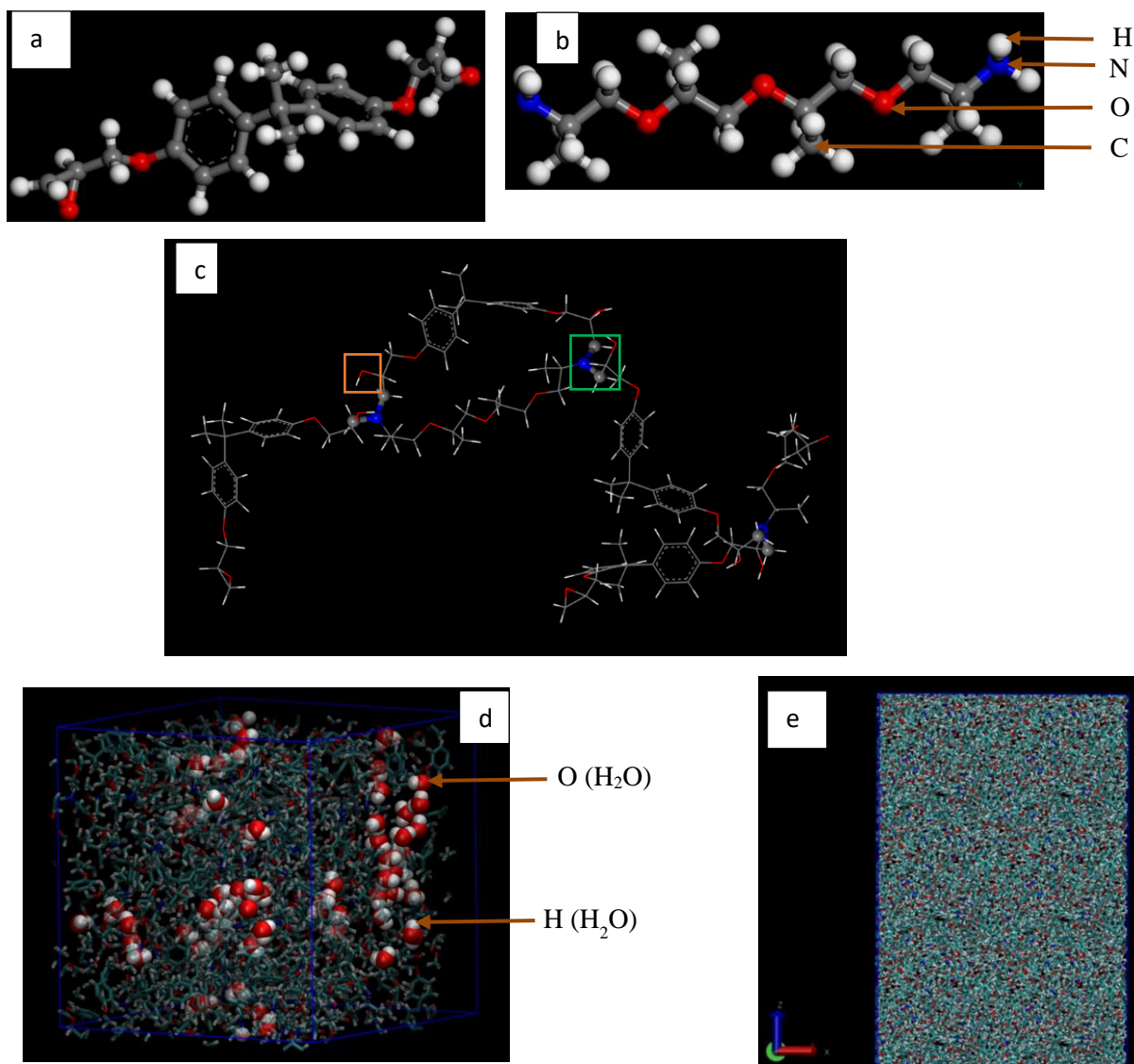


Figure 1: a) Molecular structure of DGEBA epoxy polymer, b) molecular structure of JD230 as curing agent, c) a cross-linked fragment showing the newly formed C-N (green box) and –OH groups (orange box), d) a representative epoxy network of 72% CL with inserted water molecules. The system is periodic in all directions. The system dimension: $38.10 \text{ \AA} \times 38.10 \text{ \AA} \times 38.10 \text{ \AA}$ and the total number of atoms are 5843. e) a larger system of the epoxy network to perform the tensile test of dry epoxy sample. The system is periodic in all directions. System dimension: $76.16 \text{ \AA} \times 76.16 \text{ \AA} \times 114.242 \text{ \AA}$ and the total number of atoms are 68640.

We used Packmol software [36] to insert 1, 2 and 3 weight percentage (wt%) of water molecules in the epoxy network to represent different stages of hygroscopic aging. A representative snapshot of the hydrated epoxy network is presented in Figure 1(d). Furthermore, we used the LAMMPS [37] code to perform MD simulation in order to observe the epoxy water association. In this MD study, we utilized the standard OPLS-AA (optimized potentials for liquid simulations-all atom) force field parameters to model bonded and non-bonded interactions in the epoxy network [38]. It is important to mention that we switched from

COMPASS to OPLS-AA force field because the OPLS-AA parameters are publicly and widely available and the functional forms are simple. For water, we used the F3C force field, which was widely used to capture the dynamics of water molecules in polymeric membranes as well as nano-channels [39-41]. The equations of motion were integrated using the velocity-Verlet algorithm [42] with a time step of 0.5 fs at 300K temperature. For the NVT and NPT MD simulations, the Bussi thermostat and Nose–Hoover barostat were used [43-45]. For the tensile test, we considered a larger system to reduce the boundary effects as presented in Figure 1 (e). We used the “fix deform” command in LAMMPS to perform tensile tests with a strain rate of 10^9 s^{-1} .

To determine the bond breaking sites of the epoxy network, density functional theory (DFT)-based molecular dynamics (DFT-MD) simulations were performed. These DFT-MD simulations studied a 37-atom simplified model of the polymer solvated with 64 water molecules for a total of 229 atoms. The polymer consisted of a single chain connected to itself through periodic boundary conditions in one direction and contained at least one instance of each reactive site of interest, including amines, C-O-C ether linkages, and aromatic rings. In doing so, we have used this ideal system to help bound the energetics of polymer chain scissions at different reaction sites. In addition, use of periodicity allowed the imposition of arbitrary strain on the polymer. The DFT-MD simulations were performed with the VASP code [46-48] using projector-augmented wave function (PAW) pseudopotentials [49, 50] and the Perdew-Burke-Ernzerhof (PBE) exchange correlation functional [51]. We have sampled the Γ -point of the Brillouin zone, only, with normal planewave accuracy settings. The total imposed strain on the system was up to 20% using a timestep of 0.25 fs.

For our DFT-MD calculations, we estimated the work function of hydrolytic scission by performing NVT-MD simulations where we imposed a fixed strain on the system with one water molecule constrained to a distance between 1.15-4.0 Å from a given reaction site. These calculations were performed in the NVT ensemble with the temperature set to 400 K to help promote efficient sampling. In each simulation cell, all the atoms were free to move except for the oxygen atom of the closest water molecule and one of the atoms of the polymer reaction site (e.g., the O in the C-O-C linkage or nitrogen in the primary amine group). The DFT-MD simulations were run for a total of 2 ps each and average values were obtained over the last 1.5 ps to evaluate the average energy of the system.

Experimental

DGEBA polymerization in experimental samples

DGEBA-based epoxy resins were synthesized via the addition of epichlorohydrin and bisphenol A. Therefore, oligomers with a relatively narrow distribution of polymerization degrees were frequently obtained with a polymerization degree that was typically 0.2. On this

basis and considering that the average degree, n , is in the range of 0.1-0.2 in experimental research, a value of $n=0$ is a reasonable approximation. To further justify the DGEBA molecular model adopted with $n=0$, thermoset samples were prepared using a commercially available resin with $n=0.1$. The bulk samples were then used to measure the glass transition temperature (T_g) by employing dynamic mechanical analysis (DMA) analyses. The DMA analysis plot is provided in Figure 3 in the supplementary section. The experimentally observed T_g was 91.1° C.

It is important to mention that we also performed classical MD simulations to model the change of the thermoset's density as a function of temperature as presented in Figure 2 in the supplementary section. To ensure that the cross-linked model system sampled both glassy and rubbery states, the modeling temperatures ranged from 200 to 600 K. The MD simulated T_g was 88 °C for the cross-linked adhesive modeled structure, which is very close to the experimental value of 91.1 °C. Therefore, we can say that our choice of a DGEBA monomer, $n=0$, is justified.

Vibrational spectroscopy

In addition to atomistic simulations, we performed near-infrared spectroscopy (NIR) and mid-infrared spectroscopy (MIR) on experimentally synthesized epoxy adhesive films to gain physical insights on interactions between epoxy adhesive and water molecules. NIR spectra were acquired using a commercial FT-NIR instrument equipped with a diffuse reflectance fiber optic probe. A resolution of 16 cm^{-1} between 12000-4000 cm^{-1} was chosen with a 40 kHz velocity scanning rate over 128 scans for each acquired spectrum. Raw spectra were pre-processed using extended multiplicative scattering correction (EMSC) in the wavelength region between 7600-5500 cm^{-1} . An additional 5-point Savitzky-Golay second-derivative treatment was used to improve resolution of the amine region between 6650-6250 cm^{-1} . Spectra provided in this work (Figure 3) represent an average of 10 measurements collected across various regions of the epoxy adhesive sample (pre-soaked and soaked) as described above in order to improve the representativeness of the acquired data. For the MIR measurements, both the presoak and post soak samples were analyzed using the Perkin Elmer Spectrum One C20470 instrument with Durascope accessory and a diamond crystal. All background and sample spectra were acquired using 16 scans and scanning from 4000-650 cm^{-1} with a resolution of 4 cm^{-1} .

Experimental tensile tests

We performed tensile tests on the epoxy adhesives under dry and wet conditions to study the mechanical properties. After curing, the synthesized adhesive films were cut to 12.7mm x 177.8mm strips using a diamond cutter. Prior to submerging the samples in DI water, each was measured for weight, thickness, and width. The averages of these values were recorded as 2.5g in weight, 1.06 mm in thickness, and 13.3 mm in width. The length of prepared specimens was

assumed to be an average of 178 mm. Samples were grouped into quadruplicate sets, labelled, and then submerged in a sealed container of ambient temperature DI water. To obtain tensile properties of the adhesive (in both dry and wet stages), the specimens were removed from the water, padded dry and then weighed using an analytical balance. Samples were then tested at room temperature using an INSTRON model 5567 universal test machine with a load cell capacity of 30 kN, a constant pull rate of 12.5 mm/min and a 127 mm gauge length.

As a summary of the methodology section, it is important to mention a few limitations of the simulated systems with respect experimental samples. In general, very high cross-link conversions ($> 85\%$) are less likely to occur in experiments due to topological and viscosity constraints. Therefore, we simulated two epoxy systems that can tentatively mimic the higher-end cross-linked structures for instance $\sim 70\%$ cross-linked structures. Two different cross-link numbers were chosen in the higher end, such as 63% and 72% to see the impact of cross-linking percentage with water molecules association and corresponding diffusion behavior. The cross-linked simulated structure and experimental samples are not completely identical, but they were not too far apart, though as suggested by the T_g number and density. On a different note, if we had the same cross-link percentage both for simulated and experimental samples even though they will not be identical samples. For instance, in the experimental sample there will be the presence of defects but in the simulated sample, there were no defects. Therefore, it is important to mention that there are some discrepancies between the experimental and simulated samples. However, they are not too far off to capture the physics of the early stage of hygroscopic aging and their impact on mechanical properties.

Results and Discussion

Diffusion and Transport of Water Molecules into Polymer Networks

When water molecules penetrate the bulk interior of cross-linked polymers, they produce certain physical and chemical changes to the polymer. Moisture, therefore, poses a great challenge to epoxy resin-based adhesives and understanding the dynamics of water molecules entering the epoxy matrix is pivotal. The diffusion coefficient (D) of water molecules inside the epoxy network was calculated from the mean square displacement (MSD) curve by employing the Einstein equation [52]. The MSD curve of water molecules on different hydrated systems is presented in Figure 4 in the supplementary section. Table 1 contains the D values of water molecules in epoxy adhesive as a function of water content. Our calculations show that the water diffusion coefficient was approximately two orders of magnitude lower than the bulk diffusivity of water. The movement of bulk water molecules and water molecules inside the cross-linked polymer network are significantly different. For instance, water molecules stay in the free volume of the cross-linked polymer network. Therefore, water molecules face steric hindrance

due to the presence of polymer chains and different functional groups present in the chain [53]. There might be a possibility that the water molecules may form hydrogen bonds with the functional groups i.e, hydroxyl groups and amine groups and hence the D values of water molecules become lower compared to bulk water molecules. Water immersion gravimetric experiments were performed to acquire an empirical diffusion coefficient of $8.84 \times 10^{-10} \text{ cm}^2/\text{s}$. The experimentally measured diffusion coefficient is three orders of magnitude lower compared to simulated diffusion coefficients. These discrepancies might be due to the nature of the complex cross-linked structures presented in real life experimental samples, which is difficult to mimic exactly by employing classical MD force fields. However, the employed force field can capture the slower dynamics of water molecules inside cross-linked epoxy networks. Additionally, the D values increases with increasing water content for both cross-linked structures except for 1wt% water content for 72% cross-linked structure. Limited water-polymer interaction sites in capable of forming hydrogen bonds in the MD systems might be the reason for this type of inconsistent trends in the D values.

Table 1: Diffusion coefficients for water molecules in epoxy adhesive systems. For comparison, the bulk diffusivity of water molecules is $2.9 \times 10^{-5} \text{ cm}^2/\text{s}$ at room temperature [54].

| %CL | % Water | D ($10^{-7} \text{ cm}^2/\text{s}$) |
|-----|---------|---------------------------------------|
| 63 | 1 | 0.54 |
| | 2 | 1.45 |
| | 3 | 1.61 |
| 72 | 1 | 2.07 |
| | 2 | 1.26 |
| | 3 | 1.57 |

Hydrogen-Bonding Interactions between Water and Epoxy Adhesives

Water uptake introduces changes to the epoxy structure and loss of mechanical strength [55-57]. In order to characterize structural changes, we determined the radial distribution function (RDF) among key atoms of the epoxy network and water molecules as presented in Figure 2. Additionally, to study the hydrogen-bonding environments in soaked and presoaked epoxy network and to compare our conclusions from the calculated RDFs, we utilized empirical NIR and MIR spectroscopy. The spectra are presented in Figure 3. To obtain meaningful physical insights regarding the structural changes due to water uptake by comparing experimental samples and epoxy model systems, the two systems have to be similar enough. The extent of the conversion depends very much on the curing protocol, time and temperature. In general, very high cross-link conversions ($> 85\%$) are less likely to occur in experiments due to

topological and viscosity constraints. In our particular experimental case, thermosets were cured at 70°C for about 2 hours in order to make bulk adhesive samples for mechanical and moisture uptake tests. On this basis, it is reasonable to expect that some epoxy groups did not react. This is in agreement with the characteristic absorption of C-O-C for epoxy groups observed at 930 cm⁻¹ as presented in Figure 3 (a). Similar to the experimental sample our cross-linked molecular epoxy models had small amounts of unreacted epoxy groups. In addition to that the simulated T_g value (88°C) was very close to the experimental T_g value (91°C). Therefore, we believe the molecular model with some unreacted epoxy groups presented in this work is representative of a cross-link conversion for this particular combination of resin, curing agent, and processing conditions. It is important to mention that there is a short absorption band around 3450 cm⁻¹ displayed in Figure 3a. This short broad band is assigned to O-H stretching of water hydroxyl groups [58], revealing the presence of some moisture after the drying process, where we used rather conservative temperatures due to the relatively low T_g. We are not ruling out any presence of OH groups in the resin's backbone. We rather assume very low numbers of those OH groups considering the average polymerization degree as well as the experimental conditions of temperature.

From the RDFs it is clear that for all cases (Figure 2 (a-j)) there is an association between water molecules and parts of the epoxy polymer around 2 Å distance. This association is comparable to hydrogen bonding between the epoxy polymer and water. In the epoxy model system, the hydrogen bonding acceptor can be either nitrogen or oxygen and the donor can be any hydrogen atom linked to an electronegative atom, such as nitrogen or oxygen (e.g., amine or hydroxyl). The RDFs calculated from MD clearly show a strong association with hydroxyl groups (Figure 2 (b, g)), as well a small probability of water at the C-O-C ether site, (H-OS RDF at Figure 2 (e, j)). This ether interaction is consistent with the decreased intensity of MIR bands centered at 1230 and 1030 cm⁻¹ in the spectra presented in Figure 3 (a) [59]. Additionally, it is evident that water molecules are strongly associated with nitrogen atoms in the epoxy system as presented in Figure 2 (a, c, f, h). The nitrogen atoms are divided into three groups, namely primary amine (-0.893e), secondary amine (-0.727e) and tertiary amine (-0.561e). Differences in partial charges on nitrogen atoms should have an impact on the RDF with water molecules. Therefore, we further studied the RDF between different nitrogen atoms and water molecules as presented in Figure 4. From Figure 4 it is clear that mainly primary and secondary amines in the epoxy polymer strongly coordinate with water molecules. In the experimental adhesive samples, these amines are also observed to participate in hydrogen bonding interactions with water molecules as evident from the NIR spectra (Figure 3b). For this epoxy adhesive system, the spectral region from ~7600-6200 cm⁻¹ contains intensity from C-H second-order combination bands (~7400-6800 cm⁻¹), the secondary hydroxyl O-H overtone from reacted

epoxy groups ($\sim 7000\text{ cm}^{-1}$) [60, 61], and primary/secondary amine N–H overtones ($\sim 6470\text{ cm}^{-1}$) [62]. A broad combination band from water O–H symmetric and asymmetric stretches ($\nu_1 + \nu_3$) is also convoluted in this region. In order to more clearly observe the water-amine interactions, second-derivative ($d^2/d\lambda^2$) spectra of the amine region were calculated in Figure 3b. Upon soaking, the $d^2/d\lambda^2$ spectra clearly illustrate a red-shift of the higher-energy amine stretches at $\sim 6510\text{ cm}^{-1}$, leading to greater intensity in the lower-energy $\sim 6460\text{ cm}^{-1}$ band. Although interactions between hydroxyl and water are also anticipated, these vibrational shifts are challenging to deconvolute without overfitting, given the overlap of multiple vibrational contributions.

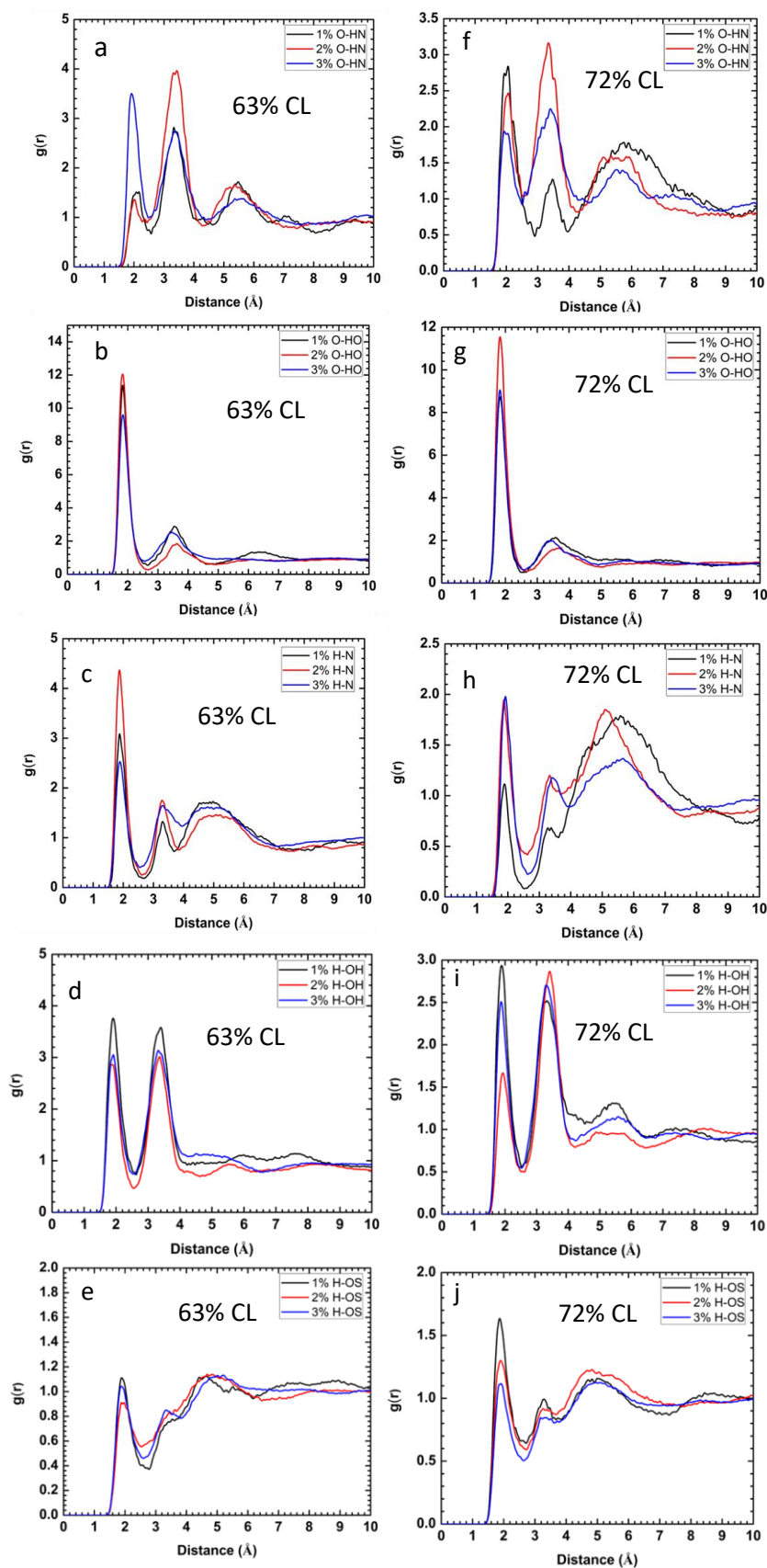


Figure 2: RDF between epoxy polymer and water. a) O-HN, b) O-HO, c) H-N, d) H-OH and e) H-OS coordination for 63% cross-linking system. f) O-HN, g) O-HO, h) H-N, i) H-OH and j) H-OS coordination for 72% cross-linking system. Here, H = H atom in water, O = O atom in water, N = N atom in polymer, HN = H atom of amine group in polymer, HO = H atom of hydroxyl group in polymer, OH = O atom of hydroxyl group in polymer, OS = O atom of ether group in polymer.

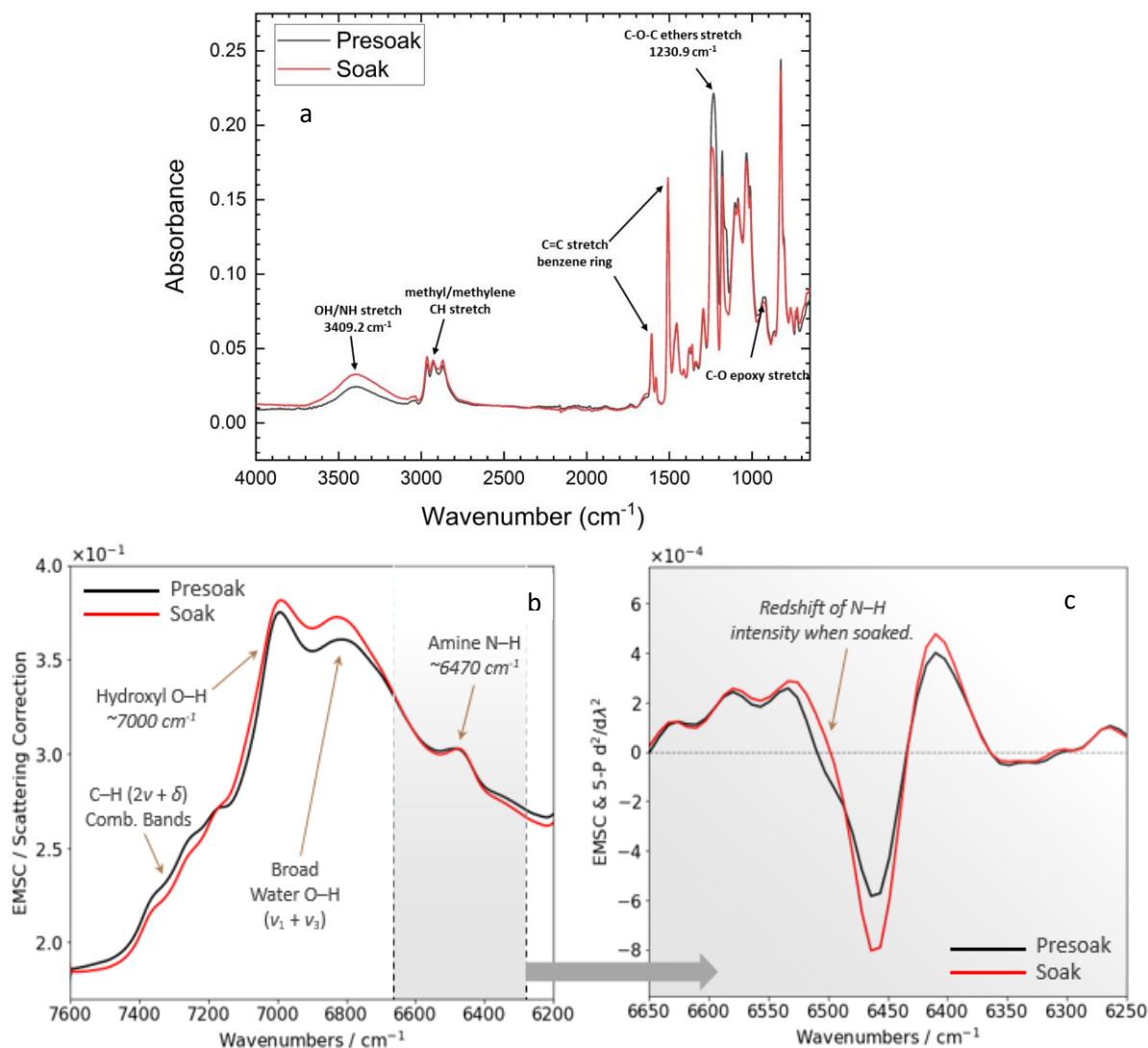


Figure 3: Infrared spectra of presoaked and soaked epoxy adhesive, (a) MIR spectra, (b) NIR spectra with Extended Multiplicative Scattering Correction (EMSC) treatment, (c) additional second-derivative ($d^2/d\lambda^2$) treatment of the primary and secondary amine overtone region to elucidate subtle redshift from hydrogen-bonding.

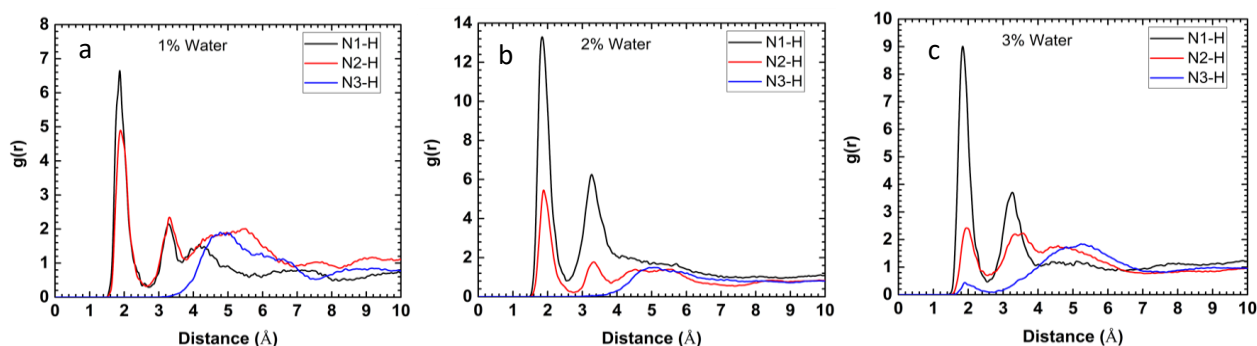


Figure 4: RDF between N atoms of epoxy polymer and hydrogen atoms of water. a) N1-H, b) N2-H and c) N3-H coordination for 63% cross-linking system. Here, N1 = primary nitrogen,

N2 = secondary nitrogen and N3 = tertiary nitrogen. Not shown here, N atoms of 72%CL epoxy system have similar RDF with water molecules.

Degradation of Epoxy Adhesive Cross-Linking with Hygroscopic Aging

Based on RDFs and vibrational spectra, the functional groups in epoxy adhesives, including hydroxyls, primary and secondary amines, and ether groups, were all found to participate in hydrogen-bonding interactions with absorbed water molecules. We hypothesize that, due to hygroscopic aging, these associations with water molecules can introduce hydrolysis into the epoxy network, which will increase with temperature. Hydrolysis can lead to the production of small molecules and cleavage/fracture of backbones depending on the location of the reaction. From a polymer design perspective, it is important to understand which sites in the epoxy network are labile over long-term hygroscopic aging. Insights from the RDFs and vibrational spectra served as inputs for DFT-MD based calculations of the local chemistry.

Constrained reaction site DFT-MD simulations between a water molecule and both the ether and the amine sites (mainly primary amine) were performed. Our efforts with DFT have been focused on determining local chemical effects that will pertain to bond scission specifically. It was reported that the initial chain scission chemistry is largely local, and depends on the nearest neighbor interactions, only [63]. Hence, in turns of initial chemistry such as chain scissions short-length chains (i.e only 37 atoms chain in this case) are very reasonable representations of larger systems. As such, we choose to approximate chain scission as a function of tensile load by our small chain studies. This also helps to alleviate the computational burden associated with DFT calculations. It is important to mention that we imposed a fixed strain on the system with one water molecule constrained to a distance between 1.15-4.0 Å from a given primary amine and ether site. Previous literature has shown controlling the water-chain moiety distance is sufficient for computing reliable work functions for chain scission [63]. This is in part because our calculations are not static, but rather are run at finite temperature (400K). Thus, additional degrees of freedom in the system such as those of the polymer backbone are averaged over during the DFT-MD simulation. Here, we saw no strong difference in chemical rupture reactions for highly strained systems and we thus limit our discussion to strains of 10% only for the sake of brevity. We note that, in our calculations, chain scission did not occur at 10% strain in the absence of water. For the NH site, chain scission only occurred when the N-O distance was at its sampled minimum of 1.15 Å. This resulted in a spike in the energy (~ 10.5 eV) for the smallest constrained distance as presented in Figure 5. As indicated by the RDF, such a close approach is highly improbable and occurs with high energy cost, which appears to indicate that the primary amine is an unlikely rupture site. In contrast, for the C-O-C site, the polymer fragment broke when at constrained distances between 1.76 and 2 Å (in Figure 5 this is the 4th smallest distance). Results shown in Figure 5 combined with the RDFs shown in Figure 2

indicate that these bond distances, as well as the energetics, make the C-O-C ether site much more likely to be involved in chain scission.

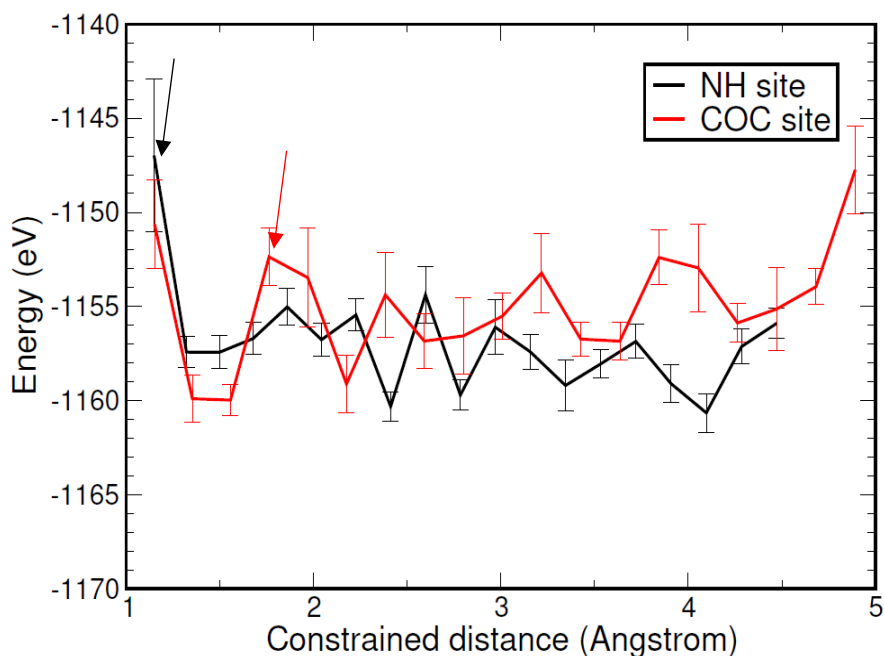


Figure 5: Energy vs. constrained distance from DFT-MD simulations. Error bars were computed as the standard deviation over each constrained simulation. Arrows indicate points at which chain scission occurred.

The goal of our efforts here is to compare the likelihood qualitatively that the C-O-C moiety will experience chain scission before the NH moiety discussed in the manuscript. In our calculations, we observed that the C-O-C moiety exhibited a net increase in system energy and bond breaking at relatively larger distances from the incoming water molecule, and the NH moiety appeared to require a much closer approach for a similar effect. This indicates the possibility that C-O-C is a more likely source for scission reactions. We plan to compute these interactions with ensemble averaging and advanced sampling approaches [63] (e.g., steered MD) in future work. From this discussion, it is evident that adhesive designers should pay attention to ether sites as a potential weak point for introducing chain scission during hygroscopic aging.

Molecular Dynamics of Tensile Properties in Epoxy Adhesives

In experiments, water uptake swells polymers, which weakens the intermolecular interactions. This is known as the plasticization effect and is known to lead to polymer degradation [64]. In the polymer membrane industry, it is understood that separation membranes

lose their molecular sieving ability because of the plasticization effect [64]. In the packaging sector the problem is delamination and induced corrosion. Water absorption degrades the mechanical strength of epoxy adhesives. To study the impact of hygroscopic aging on epoxy adhesive, we performed MD simulations of tensile tests of 63% cross-linked epoxy structure without water and hydrated epoxy structure with 1, 2 and 3 wt.% water contents. The simulated stress strain curve is presented in Figure 5 in the supplementary section and the calculated Young's modulus of dry and hydrated epoxy is presented in Figure 6.

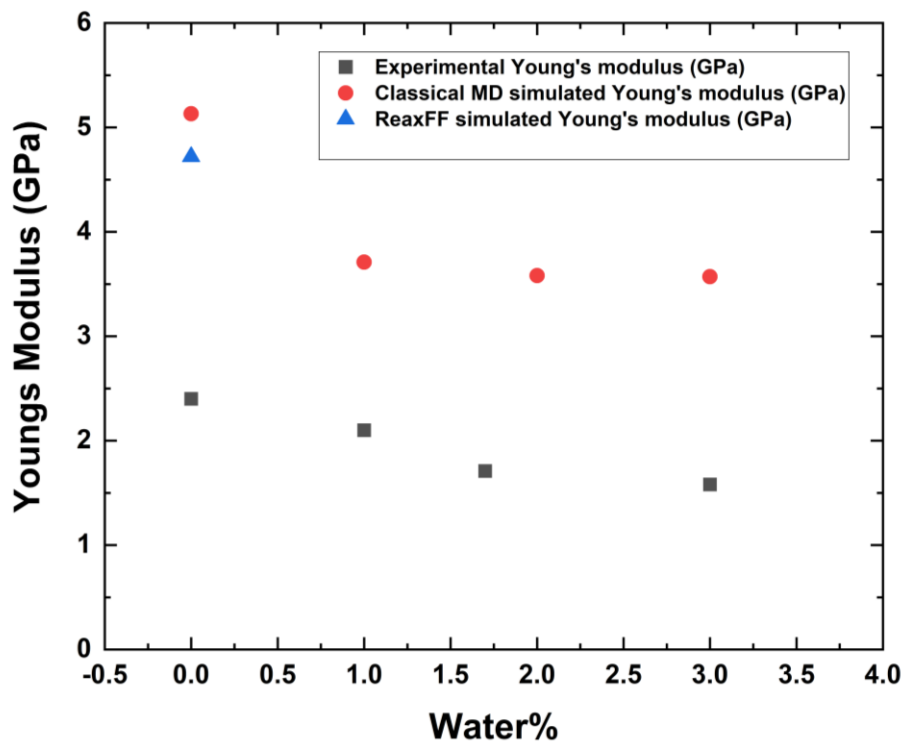


Figure 6: Measured mechanical properties of dry and hydrated 63% cross-linked structure. The Young's modulus for ReaxFF is taken from a published study [25].

The simulated Young's modulus of the dry 63% cross-linked structure is ~5 GPa, whereas the experimentally measured Young's modulus is 2.26 GPa. We need to bear in mind that the simulation cell was a simplified and ideal representation of the experimental samples. Additionally, the simulation used a strain rate that was many orders of magnitude higher than the experimental rate. Moreover, there is a possibility of the presence of humidity to the "dry" experimental sample, whereas the MD sample is by construction truly dry in the case of 0 % water. As a result of these discrepancies, we might indeed expect differences in the magnitude of mechanical properties. Our simulated Young's modulus value is comparable with a previously published value of 4.72 GPa where ReaxFF force field was used by the authors [25].

Despite these differences, the primary value of these simulations lies in identifying trends in the performance of the epoxy under different conditions and the underlying mechanisms. The decreasing trend of Young's modulus with increasing water content agrees with the experimental results. Our simulated stress-strain data indicates that increasing water content degrades the mechanical properties as presented in Figure 6. For instance, the Young's modulus decreased by ~30% with increasing water content up to 3 wt.%. It is important to mention that the degradation of mechanical property with water uptake illustrates that mitigation strategies must be considered during design of epoxy adhesive for long-term retention of adhesive properties for engineering applications.

Conclusions

We developed a molecular model to capture the dynamics and association of water molecules in epoxy adhesive. Water movement was hindered by the presence of functional groups in the epoxy polymer network. By characterizing the RDF between epoxy and water molecules, we found that hydroxyl groups, primary amines and secondary amines were the most active sites for hydrogen bond formation. The absorbed water molecules around these groups can introduce hydrolysis with hygroscopic aging. DFT-based MD simulations indicated that the ether site is likely to be the site where the chain breaks under hydration. To examine the hygroscopic aging effect on mechanical properties, we simulated tensile tests for different water content. The Young's modulus decreased by ~30% with increasing water content up to 3 wt.% in agreement with experimental data. Finally, we recommend that epoxy adhesive designers should pay attention to the percentage of cross-linking, amount of unreacted primary/secondary amines and ether groups/ethoxylated amines to prevent hygroscopic aging for long term engineering applications. This integration of high-performance computing and experiments to connect molecular level chemistry with mechanical property changes in the hydrated epoxy system presents a new direction in developing better water-resistant epoxy adhesives.

Author contributions

M. F. N. Taufique and Martin Losada have equal contribution as first author. M. F. N. Taufique performed MD simulations, analyzed the results, and wrote the manuscript. Martin Losada built monomer molecular models of epoxy and curing agents, constructed the cross-linked models and performed MD simulations with different crosslinking densities. M. J. DiTucci performed analysis of NIR spectral data and L. Pagnotti, D. Willis, and M. Torres acquired MIR and NIR data, respectively. Nir Goldman and Sebastien Hamel performed DFT-MD calculations. Ram Devanathan provided technical expertise to MD simulated data, interpreted the results, and reviewed the manuscript.

Declaration of competing interest

The authors declare no competing interest.

Acknowledgment

This work was supported by the High-Performance Computing for Energy Innovation (HPC4EI) Initiative, managed by US Department of Energy's Office of Energy Efficiency and Renewable Energy (EERE). The project was funded by EERE Vehicle Technologies Office. Pacific Northwest National Laboratory is operated for the U.S. Department of Energy by Battelle under Contract DE-AC06-76RLO1830. This research used resources of the National Energy Research Scientific Computing Center (NERSC), a U.S. Department of Energy Office of Science User Facility located at Lawrence Berkeley National Laboratory, operated under Contract No. DE-AC02-05CH11231.

Data Availability

The data that support the findings of this study are available from the corresponding author upon reasonable request.

Declaration of competing interest

The authors declare no competing interest.

References

1. May, C.A., *Introduction to epoxy resins*. Epoxy Resins Chemistry Technology, 1988: p. 1-8.
2. Soles, C.L., et al., *Contributions of the nanovoid structure to the moisture absorption properties of epoxy resins*. Journal of Polymer Science Part B: Polymer Physics, 1998. **36**(17): p. 3035-3048.
3. Mathew, J., J. Joy, and S.C. George, *Potential applications of nanotechnology in transportation: A review*. Journal of King Saud University-Science, 2019. **31**(4): p. 586-594.
4. Beardmore, P. and C. Johnson, *The potential for composites in structural automotive applications*. Composites Science and Technology, 1986. **26**(4): p. 251-281.
5. Lyu, M.-Y. and T.G. Choi, *Research trends in polymer materials for use in lightweight vehicles*. International journal of precision engineering and manufacturing, 2015. **16**(1): p. 213-220.
6. Arafat, Y., I. Dutta, and R. Panat, *On the deformation mechanisms and electrical behavior of highly stretchable metallic interconnects on elastomer substrates*. Journal of Applied Physics, 2016. **120**(11): p. 115103.
7. Arafat, Y., I. Dutta, and R. Panat, *Super-stretchable metallic interconnects on polymer with a linear strain of up to 100%*. Applied Physics Letters, 2015. **107**(8): p. 081906.
8. Patel, V. and Y. Mahajan, *Polymer nanocomposites: emerging growth driver for the global automotive industry*, in *Handbook of polymernanocomposites. Processing, performance and application*. 2014, Springer. p. 511-538.
9. Ratna, D., *Handbook of thermoset resins*. 2009: ISmithers Shawbury, UK.
10. Lee, H. and K. Neville, *Handbook of epoxy resins*. 1967.
11. Barton, J.M., *The application of differential scanning calorimetry (DSC) to the study of epoxy resin curing reactions*. Epoxy resins composites I, 1985: p. 111-154.
12. Meyer, F., et al., *The effect of stoichiometry and thermal history during cure on structure and properties of epoxy networks*. Polymer, 1995. **36**(7): p. 1407-1414.
13. Chen, X. and B. Ellis, *Coatings and other applications of epoxy resins*, in *Chemistry and technology of epoxy resins*. 1993, Springer. p. 303-325.
14. Pandiyan, S., et al., *A molecular dynamics study of water transport inside an epoxy polymer matrix*. Computational Materials Science, 2015. **106**: p. 29-37.
15. Yang, S., et al., *Molecular dynamics and micromechanics study of hygroelastic behavior in graphene oxide-epoxy nanocomposites*. 2019. **164**: p. 425-436.
16. Park, H., et al., *Prediction of quasistatic constitutive equations of moisture-absorbed epoxy polymers using atomistic simulations*. Extreme Mechanics Letters, 2020. **41**: p. 100983.

17. Kwon, S., M.Y. Lee, and S. Yang, *Molecular dynamics approach on the hygroelastic behavior of epoxy/graphene nanocomposites*. Journal of Mechanical Science Technology, 2019. **33**(2): p. 741-747.
18. Asp, L., *The effects of moisture and temperature on the interlaminar delamination toughness of a carbon/epoxy composite*. Composites Science and Technology, 1998. **58**(6): p. 967-977.
19. O'BRIEN, T.K., *Delamination of composite materials*, in *Composite Materials Series*. 1991, Elsevier. p. 181-198.
20. Krakovský, I., et al., *Structure and swelling behaviour of epoxy networks based on α , ω -diamino terminated poly (oxypropylene)-block-poly (oxyethylene)-block-poly (oxypropylene)*. Polymer, 2005. **46**(1): p. 109-119.
21. Krakovský, I., J. Pleštil, and L. Almásy, *Structure and swelling behaviour of hydrophilic epoxy networks investigated by SANS*. Polymer, 2006. **47**(1): p. 218-226.
22. Carfagna, C., A. Apicella, and L. Nicolais, *The effect of the prepolymer composition of amino-hardened epoxy resins on the water sorption behavior and plasticization*. Journal of Applied Polymer Science, 1982. **27**(1): p. 105-112.
23. Botelho, E.C., et al., *A review on the development and properties of continuous fiber/epoxy/aluminum hybrid composites for aircraft structures*. Materials Research, 2006. **9**(3): p. 247-256.
24. Pecht, M., *A model for moisture induced corrosion failures in microelectronic packages*. IEEE transactions on components, hybrids, and manufacturing technology 1990. **13**(2): p. 383-389.
25. Chowdhury, S.C., et al., *Epoxy resin thermo-mechanics and failure modes: effects of cure and cross-linker length*. Composites Part B: Engineering, 2020. **186**: p. 107814.
26. Ogata, S. and M. Uranagase, *Unveiling the chemical reactions involved in moisture-induced weakening of adhesion between aluminum and epoxy resin*. The Journal of Physical Chemistry C, 2018. **122**(31): p. 17748-17755.
27. Nizin, D.R., et al. *Natural Climatic Aging of Epoxy Polymers Taking into Account the Seasonality Impact*. in *Key engineering materials*. 2019. Trans Tech Publ.
28. Uthaman, A., et al., *Durability of an epoxy resin and its carbon fiber-reinforced polymer composite upon immersion in water, acidic, and alkaline solutions*. Polymers, 2020. **12**(3): p. 614.
29. Ulus, H., et al., *Halloysite nanotube reinforcement endows ameliorated fracture resistance of seawater aged basalt/epoxy composites*. 2020. **54**(20): p. 2761-2779.
30. Ogata, S. and Y.J.T.J.o.P.C.C. Takahashi, *Moisture-induced reduction of adhesion strength between surface oxidized Al and epoxy resin: dynamics simulation with electronic structure calculation*. The Journal of Physical Chemistry C, 2016. **120**(25): p. 13630-13637.
31. Ogata, S. and M.J.T.J.o.P.C.C. Uranagase, *Unveiling the chemical reactions involved in moisture-induced weakening of adhesion between aluminum and epoxy resin*. 2018. **122**(31): p. 17748-17755.
32. Sun, H., P. Ren, and J. Fried, *The COMPASS force field: parameterization and validation for phosphazenes*. Computational and Theoretical Polymer Science, 1998. **8**(1-2): p. 229-246.
33. Meunier, M. *Introduction to materials studio*. in *EPJ Web of Conferences*. 2012. EDP Sciences.
34. Bandyopadhyay, A., et al., *Molecular modeling of crosslinked epoxy polymers: The effect of crosslink density on thermomechanical properties*. Polymer, 2011. **52**(11): p. 2445-2452.
35. Masoumi, S., B. Arab, and H.J.P. Valipour, *A study of thermo-mechanical properties of the cross-linked epoxy: An atomistic simulation*. Polymer, 2015. **70**: p. 351-360.
36. Martínez, L., et al., *PACKMOL: a package for building initial configurations for molecular dynamics simulations*. Journal of computational chemistry, 2009. **30**(13): p. 2157-2164.
37. Plimpton, S., *Fast parallel algorithms for short-range molecular dynamics*. Journal of computational physics, 1995. **117**(1): p. 1-19.
38. Jorgensen, W.L., D.S. Maxwell, and J. Tirado-Rives, *Development and testing of the OPLS all-atom force field on conformational energetics and properties of organic liquids*. Journal of the American Chemical Society, 1996. **118**(45): p. 11225-11236.
39. Levitt, M., et al., *Calibration and testing of a water model for simulation of the molecular dynamics of proteins and nucleic acids in solution*. The Journal of Physical Chemistry B, 1997. **101**(25): p. 5051-5061.
40. Devanathan, R., A. Venkatnathan, and M. Dupuis, *Atomistic simulation of nafion membrane: I. Effect of hydration on membrane nanostructure*. The Journal of Physical Chemistry B, 2007. **111**(28): p. 8069-8079.
41. Shin, Y., et al., *Highly selective supported graphene oxide membranes for water-ethanol separation*. Scientific reports, 2019. **9**(1): p. 1-11.
42. Swope, W.C., et al., *A computer simulation method for the calculation of equilibrium constants for the formation of physical clusters of molecules: Application to small water clusters*. The Journal of chemical physics, 1982. **76**(1): p. 637-649.
43. Bussi, G., D. Donadio, and M.J.T.J.o.c.p. Parrinello, *Canonical sampling through velocity rescaling*. The Journal of chemical physics, 2007. **126**(1): p. 014101.
44. Nosé, S.J.T.J.o.c.p., *A unified formulation of the constant temperature molecular dynamics methods*. The Journal of chemical physics, 1984. **81**(1): p. 511-519.
45. Hoover, W.G.J.P.r.A., *Canonical dynamics: Equilibrium phase-space distributions*. 1985. **31**(3): p. 1695.
46. Kresse, G. and J. Hafner, *Ab initio molecular dynamics for liquid metals*. Physical Review B, 1993. **47**(1): p. 558.

47. Kresse, G. and J. Hafner, *Ab initio molecular-dynamics simulation of the liquid-metal–amorphous-semiconductor transition in germanium*. Physical Review B, 1994. **49**(20): p. 14251.
48. Kresse, G. and J. Furthmüller, *Efficient iterative schemes for ab initio total-energy calculations using a plane-wave basis set*. Physical review B, 1996. **54**(16): p. 11169.
49. Blöchl, P.E., *Projector augmented-wave method*. Physical review B, 1994. **50**(24): p. 17953.
50. Kresse, G. and D. Joubert, *From ultrasoft pseudopotentials to the projector augmented-wave method*. Physical review B, 1999. **59**(3): p. 1758.
51. Perdew, J.P., K. Burke, and M. Ernzerhof, *Generalized gradient approximation made simple*. Physical Review Letters, 1996. **77**(18): p. 3865.
52. Wang, J. and T. Hou, *Application of molecular dynamics simulations in molecular property prediction II: diffusion coefficient*. Journal of computational chemistry, 2011. **32**(16): p. 3505-3519.
53. Yang, C., et al., *A comprehensive review on water diffusion in polymers focusing on the polymer–metal interface combination*. Polymers, 2020. **12**(1): p. 138.
54. Mark, P. and L. Nilsson, *Structure and dynamics of the TIP3P, SPC, and SPC/E water models at 298 K*. The Journal of Physical Chemistry A, 2001. **105**(43): p. 9954-9960.
55. Lin, Y. and X. Chen, *Moisture sorption–desorption–resorption characteristics and its effect on the mechanical behavior of the epoxy system*. Polymer, 2005. **46**(25): p. 11994-12003.
56. Wunderle, B., et al. *Molecular dynamics approach to structure-property correlation in epoxy resins for thermo-mechanical lifetime modeling*. in *2009 59th Electronic Components and Technology Conference*. 2009. IEEE.
57. Pethrick, R.A., et al., *Dielectric, mechanical and structural, and water absorption properties of a thermoplastic-modified epoxy resin: poly (ether sulfone)– amine cured epoxy resin*. Macromolecules, 1996. **29**(15): p. 5208-5214.
58. Parker, F.S., *Applications of infrared, Raman, and resonance Raman spectroscopy in biochemistry*. 1983: Springer Science & Business Media.
59. Herzberg, G. and B. Crawford Jr, *Infrared and Raman spectra of polyatomic molecules*. The Journal of Physical Chemistry, 1946. **50**(3): p. 288-288.
60. Manzanares I, C., et al., *Overtone spectra of C–H bonds and vibrational abinitio study of methoxy boranes*. The Journal of chemical physics, 1991. **95**(5): p. 3031-3039.
61. Iwamoto, R., A. Nara, and T. Matsuda, *Near-Infrared Combination and Overtone Bands of the CH 2 Sequence in CH 2 X 2, CH 2 XCHX 2, and CH 3 (CH 2) 5 CH 3 and their Characteristic Frequency Zones*. Applied spectroscopy, 2006. **60**(4): p. 450-458.
62. González, M.G., J.C. Cabanelas, and J. Baselga, *Applications of FTIR on epoxy resins-identification, monitoring the curing process, phase separation and water uptake*. Infrared Spectroscopy-Materials Science, Engineering and Technology, 2012. **2**: p. 261-284.
63. Kroonblawd, M.P., N. Goldman, and J.P. Lewicki, *Chemical degradation pathways in siloxane polymers following phenyl excitations*. Physical Chemistry B, 2018. **122**(50): p. 12201-12210.
64. Foreman, J.P., et al., *Thermodynamic and mechanical properties of amine-cured epoxy resins using group interaction modelling*. Journal of materials science, 2006. **41**(20): p. 6631-6638.